ACS Photonics

pubs.acs.org/journal/apchd5

Article

Femtosecond Optical-Field-Driven Currents in Few-Nanometer-Size Gaps with Hot Electron Injection into Metallic Leads

Andrei G. Borisov,* Boyang Ma, Mario Zapata-Herrera, Antton Babaze, Michael Krüger, and Javier Aizpurua

Cite This: *ACS Photonics* 2025, 12, 2137−2150

Read Online

ACCESS | Metrics & More | Article Recommendations | Supporting Information

ABSTRACT: Current nanoscale optoelectronic devices can reach femtosecond response times by exploiting highly nonlinear light−matter interactions. Shaping of the field waveform of few-cycle optical pulses allows one to control electron emission from nanotips and nanoparticles as well as to drive electron transport in ≳10 nm wide plasmonic gaps. In this work, we address the less explored optically induced electron transport in much narrower, 1−2 nm metallic gaps of interest in many practical situations such as in light-wave-driven scanning tunneling microscopy or in transduction between electrons and photons for optoelectronic applications. Using the time-dependent density functional theory, model calculations, and semiclassical electron trajectories derived from an analytical strong-field model, we bring robust evidence that the sub-cycle bursts of photoemitted electrons might cross the gap prior to the change of the sign of the optical field and thus without experiencing quiver motion. This leads to a characteristic carrier-envelope phase dependence of the net electron transport. Most importantly, we show that in the optical field emission regime, continuous acceleration of electron bursts moving in the gap by an optical field results in high electron energies. The electron current in a narrow-gap nanocircuit is then associated with hot electron injection into the metallic leads characterized by a non-thermal post-injection energy distribution. This is in contrast with electron transport through wide gaps dominated by low-energy electrons. Our results contribute to the design of optoelectronic devices operating on femtosecond temporal and nanometer spatial scales.

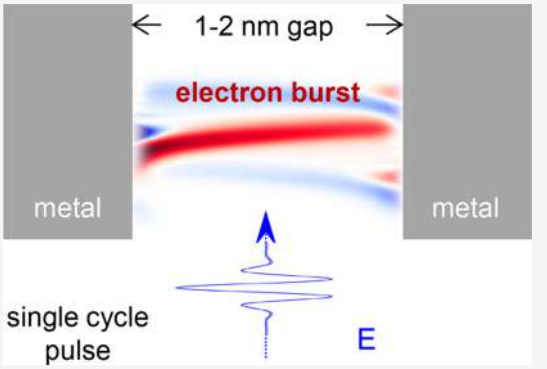

KEYWORDS: *nanojunction, single-cycle laser pulse, photon-assisted tunneling, multiphoton emission, optical field emission, TDDFT*

INTRODUCTION

Energy transfer from photons to bound electrons, followed by their excitation and eventual emission, is one of the most studied and most exploited effects in light−matter interaction. The theoretical and experimental research on this process has been further fueled by the development of phase-stabilized intense few-cycle optical pulses opening unprecedented possibilities for revealing and controlling the photoemission dynamics at time scales entering the attosecond range.[1−7] The symmetry breaking produced by the electric field of the few-cycle pulses leads to the carrier-envelope phase (CEP)-dependent asymmetry in electron emission from atoms[8−10] and nanoobjects.[11−13] Shaping the waveform of the optical pulse allows one to control induced currents in 2D and 3D materials,[14−18] as well as photoemission from metal surfaces.[19−23] In this respect, the light-driven steering of electrons from metal tips[24−31] and plasmonic nanoparticles[32−36] in the optical field emission regime provides an attosecond window into the process of electron emission and rescattering from the surface.[3,37] Among other developments, the coherent control of sub-fs electron bursts in nanocircuits holding plasmonic gaps of widths $d_{gap} \gtrsim 10$ nm has been reported in a number of studies[38−46] targeting on-chip determination of the CEP[38,40,42,45] and the full waveform of the optical transient[44,46] as well as engineering of petahertz optoelectronic devices.[47,48]

A combination of sub-fs (or even attosecond) temporal resolution provided by single-cycle optical pulses[6,7,44] with the atomic-scale spatial resolution provided by scanning probes[49] offers unprecedented perspectives in studying and controlling light−matter interaction.[50−53] Along this path, recent experimental studies addressed the coupling between an optical field and electron transport in 1−2 nm junctions of a scanning tunneling microscope (STM) and of bowtie nanoantennas.[54−59]

While reducing the size of the gap down to a few nanometers is of interest in light-wave-driven STM, and

Received: December 30, 2024
Revised: March 20, 2025
Accepted: March 21, 2025
Published: April 1, 2025

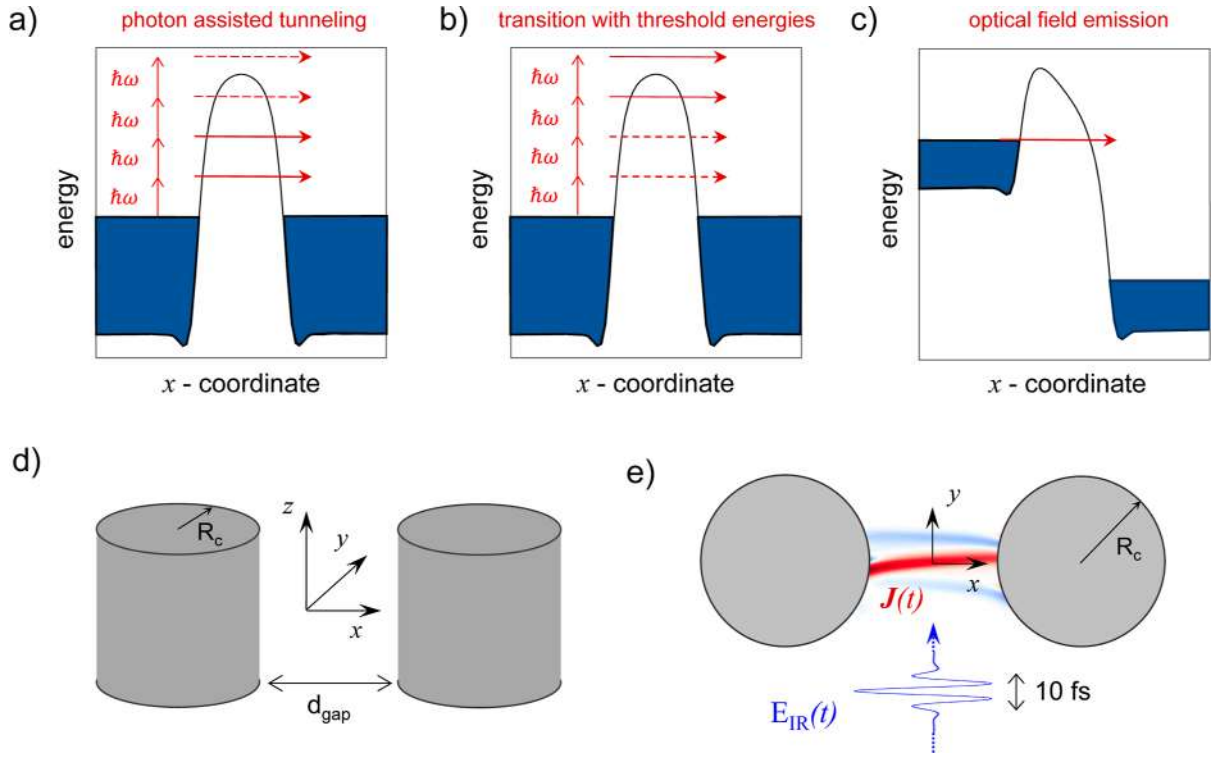

Figure 1. Sketch of the electron transport processes in the studied system. (a,b) Multiphoton regime of electron transport (weak fields). The n-photon absorption can lead to photon-assisted tunneling through the potential barrier reduced by $n\hbar\omega$ as compared to the field-free case (solid red arrows, panel a) or to the over-the-barrier and under-the-barrier transitions with energies close to the threshold given by the height of the tunneling barrier (solid red arrows, panel b). In panels (a) and (b), the dashed arrows show less probable electron transport channels. Occupied electronic states of the metal are shaded in blue. (c) Optical field emission regime (strong fields) where an electron tunnels through the potential barrier reduced by the optical field. (d) Sketch of the system of the two free-electron metal cylindrical nanowires infinite along the z-axis and separated by a narrow gap of width d_{gap} (typically 1−6 nm). The middle of the gap is located at (x = 0, y = 0). The nanowire radii are R_c = 5 nm. (e) Cross section (x, y) of the system of two parallel cylindrical nanowires shown in panel (d). The x-polarized single-cycle infrared pulse incident on the nanowires along the y-axis triggers an electron current $J(t)$ across the gap. In the inset, we show the x-component of the time-dependent electric field of the pulse with frequency ω = 0.95 eV (wavelength 1300 nm), and CEP = 0.

more generally in (ultrafast) optoelectronic applications and in transduction between tunneling electrons and photons or plasmons,[57,58,60−65] an accurate theoretical description of electron transport in such systems is challenging. In particular, when electron transport is induced by few-cycle optical pulses in the multiphoton or strong-field regime. Indeed, continuous-wave theories such as the perturbative theory of photon-assisted tunneling[66,67] do not apply to situations where electron transfer across the gap involves both above- and below-barrier transitions. Note also that for symmetric geometries, the net electron transport is only possible because of the symmetry break produced by the field of the short optical pulse. The strong-field approximation (SFA) in its formulation for photoemission from metal surfaces[23] also has to be taken with care because of the field screening inside the metal, which results in an extremely short spatial range where an electron can explore the optical field. This is without mentioning the general difficulty to describe the potential barrier and the field screening for few-nanometer gaps where quantum effects such as nonlocality and spill-out of electron density[68,69] become important, as well as the difficulty to address the intermediate region of laser intensities between multiphoton and strong-field regimes.

Most of the theoretical approaches applied so far to explain optically induced electron transport in the 1−2 nm size metallic junctions are based on the solution of one-electron time-dependent Schrödinger equation[70,71] or on the strong-field approximation and semi-classical theory.[59,71,72] The stationary tunneling theory[55−58] is also evoked in this context. In all the cases mentioned previously, a model potential of the system is employed, involving an unavoidable parameterization of the electron−metal interaction, field screening, etc. Optically induced electron transport has been also addressed with many-body approaches such as the time-dependent density functional theory (TDDFT), which includes an atomistic description of the leads.[73−75] However, the cost to pay for the high computational demand of an ab initio atomistic theory is the limitation in the size of the systems and the limited range of variation of the parameters of the optical pulse that could be tackled. This points toward the opportunity and relevance of many-body calculations where a simplified, yet realistic description of the metallic valence electrons (i) allows one to gain valuable insights into the physical processes underlying electron dynamics and electron transport triggered in a narrow metallic gap by a single-cycle optical pulse in conditions relevant to actual experiments and (ii) provides a solid reference for model approaches such as the recently reported semi-analytical theory of attosecond tunneling microscopy.[71]

In this work, using TDDFT and a free-electron description of the metal, we address the challenges above. Our calculations fully account for nonlocality, spill-out of electron density, and

https://doi.org/10.1021/acsphotonics.4c02612
ACS Photonics 2025, 12, 2137−2150

self-consistent dynamical screening of the optical field in the junction. They provide the femtosecond dynamics of electron density and electron currents induced by experimentally available single-cycle optical pulses with carrier frequency $\omega = 0.95$ eV (1300 nm wavelength) in a narrow metallic gap of 1−2 nm width. The results obtained in this work demonstrate that within a broad range of field amplitudes, short electron bursts resulting from the highly nonlinear photoemission process directly cross the gap in times below a quarter of an optical period. The physical mechanisms behind the electron dynamics revealed here have implications for the optical waveform dependence of the net electron current produced across the gap as well as for the energy transfer from the optical field to photoemitted electrons resulting in hot electron injection into the metallic leads. We believe that our work advances the theoretical background necessary for (petahertz) optoelectronic applications, as well as for the development of time-resolved STM.

Atomic units (a.u.) are used throughout this paper, unless otherwise stated.

MODEL SYSTEM AND THEORETICAL DESCRIPTION OF THE ULTRAFAST ELECTRON DYNAMICS

Several processes shown in Figure 1 are of relevance for the optically induced transport in narrow metallic junctions such as those in the STM device.[4,50] For low optical fields, photon absorption can lead to photon-assisted tunneling at negative electron energies with respect to the top of the barrier (Figure 1a) or to an over-the-barrier transition (Figure 1b). For strong optical fields, the barrier lowering induced by the optical field opens the possibility for optical field emission to occur (Figure 1c).

To address and characterize these processes in a parameter-free many-body approach, we employ TDDFT calculations of the optically induced electron currents in the narrow gap of a cylindrical nanowire dimer as detailed in the Supporting Information (Section SI1). Identical parallel metallic nanowires sketched in Figure 1 have a radius $R_c = 5$ nm, infinitely extend along the z-axis, and are separated by a gap with a width d_{gap} measured along the dimer axis (x-axis). To make the TDDFT calculations for a system of this size affordable, the nanowires are described using the free-electron stabilized jellium metal (JM) approximation[76] with the work function of silver[77] $\Phi = 4.5$ eV. It has been demonstrated that while the JM does not allow one to account for atomistic effects on the geometry of the junction, or for the exact band structure of the material, it correctly captures the dynamics of valence electrons, and allows one to describe the experimental studies of multiphoton and optical field emission processes in metallic systems.[3,19,40,78]

The single-cycle x-polarized optical pulse with a free-space electric field

$$\mathbf{E}_{IR}(t) = \hat{e}_x E_0 e^{-t^2/\tau^2} \cos(\omega t + \varphi) \tag{1}$$

propagates along the y-axis. In eq 1, $\hat{e}_x$ is the unit length vector along the x-axis, φ is the CEP of the pulse, and $\tau = \frac{1}{\sqrt{2\ln(2)}}\frac{2\pi}{\omega}$. The time dependence of $E_{IR}(t)$ is shown in Figure 1e for $\varphi = 0$. We use $\omega = 0.95$ eV (1300 nm wavelength) so that $\mathbf{E}_{IR}(t)$ reproduces an experimentally available transient and allows us to link the present results with earlier studies[38,40] focused on the optical field emission regime and electron transport in wide gaps (see also Sections SI1 and SI2).

The electron dynamics in response to the incident electromagnetic pulse is obtained using the Kohn−Sham (KS) formalism of the TDDFT within the adiabatic local density approximation (ALDA)[79−81] and with the exchange−correlation kernel of Gunnarsson and Lundqvist.[82] The self-consistent real-time TDDFT calculations on the 2D spatial mesh in x- and y-coordinates allow us to obtain the time-dependent KS potential of the system that accounts for the dynamical screening of the induced field, the time-dependent electron density $\varrho(x, y, t)$, the time-dependent electron current density $\mathbf{j}(x, y, t)$, as well as the independent contribution to the latter of the KS orbitals initially localized in the nanowire at the left (right) of the junction $\mathbf{j}_{L(R)}(\mathbf{r}, t)$. Here $\mathbf{j}(x, y, t) = \mathbf{j}_L(\mathbf{r}, t) + \mathbf{j}_R(\mathbf{r}, t)$ holds. For the sake of brevity, we will refer to $\mathbf{j}_{L(R)}$ as the electron current created by the left (right) cylinder. These are the key quantities in the analysis of fs electron currents in nanometer-size gap. Thus, the net electron transfer between the nanowires per optical pulse $\mathcal{N}$ is given by

$$\mathcal{N} = \int dt\, J(t) \tag{2}$$

where $J(t)$ is the electron current per unit length through the $(x = 0, y, z)$ plane in the middle of the junction. It is given by

$$J(t) = \int dy\, \hat{e}_x \cdot \mathbf{j}(0, y, t) \tag{3}$$

Note that because of the translational invariance of the system along the z-axis, the quantities such as the net electron transfer or the total electron current through the junction are shown in figures below per 1 nm height.

While we perform the TDDFT calculations for a finite-size system, the results obtained in this way are representative of optically induced electron transport in experimentally available metallic gaps such as in STM and bowtie antenna junctions,[55−59] electro-migrated gaps,[60,61,83] or metal−insulator−metal (MIM) devices.[84−87] Indeed, because of the field enhancement, the near field of the dimer is most intense in the gap close to the dimer axis. Thus, the strongly nonlinear photoemission leading to an electron transfer between nanowires is also dominated by the gap region close to the dimer axis.[40] Considering $d_{gap} \lesssim R_c$ allows for reducing effects linked with the finite size of the emitter and collector. It follows from the TDDFT calculations (see detailed discussion in Section SI1) that (i) for small d_{gap}, the field induced by the optical pulse at the dimer axis in the free-space region of the gap only mildly varies with x, and (ii) the incident pulse is off-resonance with respect to the plasmon excitation of the dimer. In the absence of plasmon ringing, the waveform of the incident pulse is mirrored by the time dependence of the induced field in the gap, which allows us to focus the discussion on the main processes of interest for the present study.

For the discussion of the TDDFT results, we then characterize the field in the gap by its effective amplitude E_g. We obtained that within the range of the field strengths considered here, it can be represented as $E_g = \mathcal{R}E_0$, where the field enhancement $\mathcal{R} = 4.1$, 2.9, 1.8 for $d_{gap} = 1$, 2, 6 nm, respectively, is calculated from the self-consistent KS potential inside the junction on the dimer axis (see Figures S1 and S2 of the Supporting Information). Based on these results, in the simplified model approaches used below along with TDDFT,

https://doi.org/10.1021/acsphotonics.4c02612
ACS Photonics 2025, 12, 2137−2150

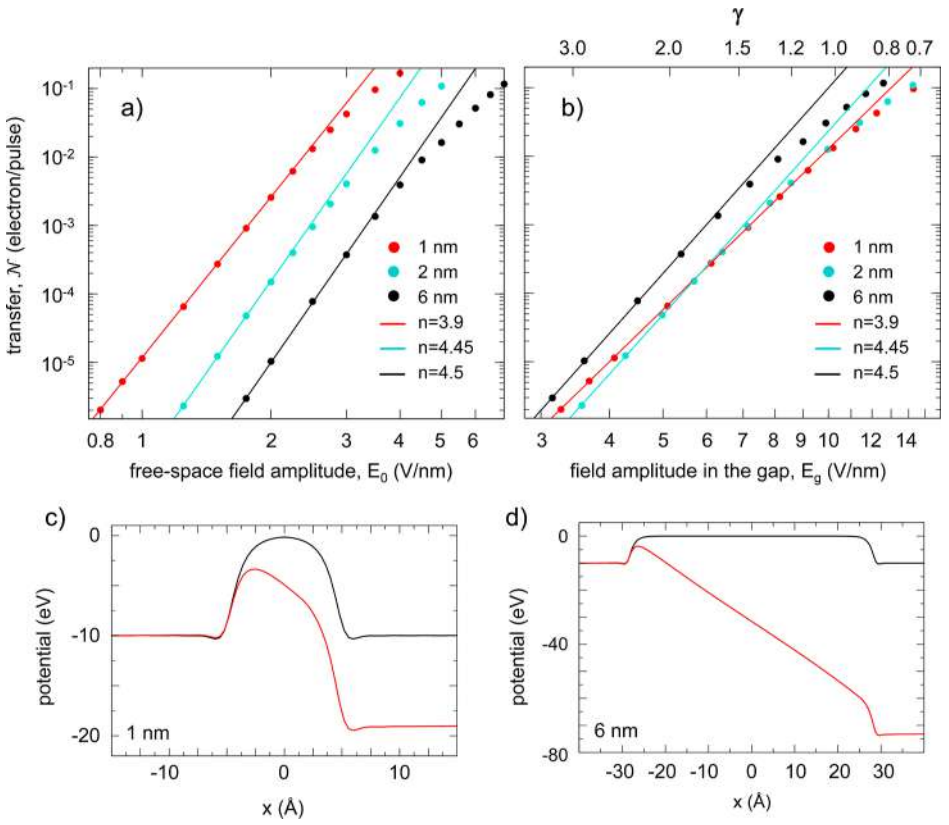

Figure 2. Multiphoton and optical field emission regime of electron transport. (a) Electron transfer $\mathcal{N}$ defined as the net number of electrons transferred per pulse across a gap of 1 nm (red), 2 nm (light blue), and 6 nm (black) width. Results of the TDDFT calculations (dots) are shown as a function of the free-space field amplitude E_0 of the incident x-polarized single-cycle pulse with CEP = π (1 and 2 nm gap) and CEP = $3\pi/4$ (6 nm gap). The lines display the fit by the $\mathcal{N} \propto E_0^{2n}$ dependence characteristic for the multiphoton regime. The number of photons n is given in the legend. (b) The same as panel (a), but results are shown as a function of the amplitude of the field in the gap E_g and of the Keldysh parameter γ. (c,d) One-electron potential in the gap region as a function of the x-coordinate along the dimer axis for the 1 nm (c) and 6 nm (d) size of the gap. The energy is measured with respect to the vacuum level. The potential of the ground-state system (black) is shown together with the time-dependent potential (red) calculated with TDDFT for the system illuminated with a CEP = π single-cycle pulse. The time-dependent potential is shown at the time instant $t = 0$ corresponding to the crest of the field with $E_g \approx 10$ V/nm. It is offset by $-E_g d_{gap}/2$ so that it converges to the ground-state potential in the bulk of the left cylinder.

the field in the gap is then considered as independent of x and it is approximated as

$$E_{gap}(t) = E_g e^{-t^2/\tau^2} \cos(\omega t + \varphi) \quad (4)$$

RESULTS

Dependence of Electron Transport on Field Amplitude. For the symmetric dimer structure considered in this work, it is solely the optical field that creates an asymmetry in electron emission from the adjacent metal surfaces across the gap leading to the net electron transfer in the system. The dependence of the net electron transfer on the optical waveform allows for disentangling various underlying physical processes[4,5,88] sketched in panels (a−c) of Figure 1.

In Figure 2a, we show the net number of electrons transferred per pulse between the nanowires, $\mathcal{N}$, calculated with TDDFT as a function of the incident field amplitude E_0. The results (dots) obtained for 1, 2, and 6 nm gaps feature the same qualitative trends. At low field strengths, we observe the multiphoton regime with an absorption of $n = 4-4.5$ photons ($\mathcal{N} \propto E_0^{2n}$). For all of the gap sizes considered here, including the 6 nm wide vacuum gap, we thus obtain that $n \approx \Phi/\omega$, where the work function Φ is the height of the vacuum barrier for electrons at the Fermi level. Therefore, we conclude that in the multiphoton regime, the electron transport corresponds to the transition with electron energies close to the top of the potential barrier separating the nanowires. For the 6 nm gap, the presence of a wide vacuum barrier imposes the over-the-barrier transitions with electron energies above the vacuum level $\mathcal{E} > 0$. For the 1 nm gap, the potential barrier is much narrower and its top is at − 0.2 eV with respect to the vacuum level. The photon-assisted tunneling with electron energy below the barrier thus becomes possible, as we show in this work. Lower barrier and electron transport involving both the over-the-barrier and under-the-barrier transitions as sketched in Figure 1b explain the lower photon order n obtained for the 1 nm gap. It is worth noting that we obtain qualitatively similar results using the JM with work function of gold (see Section SI6).

We do not observe the contribution of photon-assisted tunneling associated with one photon absorption[66] (Figure 1a), as calculated for MIM devices,[84] and experimentally observed in STM junctions or nanoantenna gaps of 1−2 nm size.[55−58] However, in these latter cases, the tunneling probability was enhanced by reducing the tunneling barrier with an applied bias, which leads to an asymmetry and thus rectification.

https://doi.org/10.1021/acsphotonics.4c02612
ACS Photonics 2025, 12, 2137−2150

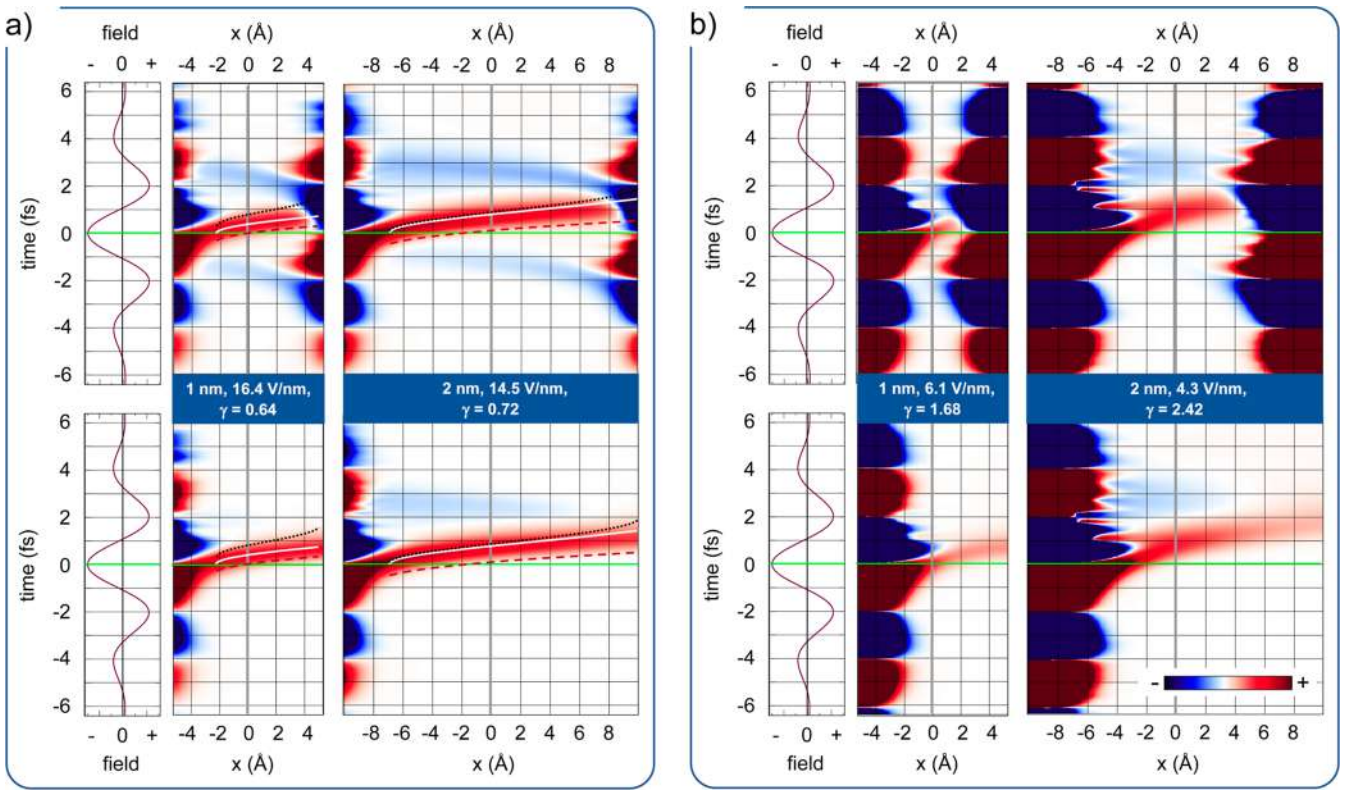

Figure 3. Dynamics of electron currents in 1 and 2 nm metallic gaps triggered by a CEP = π single-cycle optical pulse corresponding to the largest net electron transfer. The color maps display the normalized x-component of the electron current density along the dimer axis. The TDDFT results are presented as a function of x-coordinate (horizontal axis) and time (vertical axis). The color code is explained in the inset of the bottom-right panel. Top row of the subpanels: result for the complete system, $j_x(x, y = 0, t) = \hat{e}_x \cdot \mathbf{j}(x, y = 0, t)$. Bottom row of the subpanels: contribution to $j_x(x, y = 0, t)$ of the left cylinder $j_{\mathrm{L},x}(x, y = 0, t) = \hat{e}_x \cdot \mathbf{j}_{\mathrm{L}}(x, y = 0, t)$. (a) Results obtained for the optical field amplitude in the gap E_g corresponding to the onset of the optical field emission regime of electron transport. The semi-classical electron trajectories from the analytical strong-field model[71] for a 1 nm (2 nm) gap are shown with lines. Black dotted line: final electron energy $\mathcal{E}(t^*) = 0.25$ eV; white line: electron emitted at the crest of the optical field so that $\mathcal{E}(t^*) = 8.5$ eV (6.7 eV); dashed red line: electron with the cutoff energy $\mathcal{E}(t^*) = 12.8$ eV (26.3 eV). Here t^* is the time instant when the trajectory crosses the facing metal surface. (b) Results obtained for the optical field amplitude in the gap E_g corresponding to the multiphoton absorption regime of electron transport. The size of the gap d_{gap} (in nm), the field amplitude in the gap E_g (in V/nm), and Keldysh parameter γ are given with white color in the legends. The line plot at the left of each panel shows the time evolution of the electric field in the middle of the gap, $E_{gap}(t)$. Horizontal green lines: the reference time ($t = 0$) when the field in the gap reaches its extremum. Vertical gray lines mark the middle of the gap.

With increasing incident field amplitude, the TDDFT results feature lower nonlinearity than that obtained in the multiphoton regime. Such transition to lower nonlinearity at high E_0 reveals the onset of the strong-field regime.

The large quantitative differences in electron transport calculated for the same free-space field amplitude E_0 but for different d_{gap} are linked with the different enhancement of the incident field, which depends on the gap size. When presented as a function of E_g in Figure 2b, $\mathcal{N}$ obtained for gaps of different sizes fall essentially closer to each other. This result demonstrates that it is the time-dependent field in the gap that drives the electron emission and transport in the dimer. The $E_g = \mathcal{R}E_0$ introduced above appears as the relevant quantity which allows us to use the results obtained in this work for the discussion of the optically induced electron transport in narrow 1−2 nm metallic gaps in general. Thus, the optically induced transport in Figure 2b can be analyzed in terms of the Keldysh parameter[89] $\gamma = \sqrt{\Phi/2U_p}$ originally introduced to distinguish between different regimes of photoemission into the free space. Here $U_p = E_g^2/4\omega^2$ is the ponderomotive potential. The multiphoton absorption (weak fields, high nonlinearity $\mathcal{N} \propto E_g^{2n}$) corresponds to $\gamma \gg 1$. The optical field emission (strong fields, lower nonlinearity) corresponds to $\gamma \ll 1$. For the present system, we observe the transition between the two regimes at $E_g \approx 10$ V/nm ($\gamma \lesssim 1.2$), in line with experimental and theoretical studies on electron emission from surfaces, nanoobjects, and metal tips.[22,24,27,34,41,90,91]

Despite the similarity of the results obtained with different sizes of the junction, one would expect that since d_{gap} determines the spatiotemporal scale of the electron interaction with the optical field, it has a strong effect on the dynamics of the emitted electrons. To support our conjecture, we show in Figure 2c,d the ground-state potential (black line) and the dynamical potential at the crest of the optical field (red line) calculated with TDDFT for an electron moving in 1 and 6 nm wide gap of the dimer (see also Figure S2 of the Supporting Information). As expected for the length gauge and non-retarded approximation employed here, the optical field in the central part of the gap results in a linear variation of the potential with x. We observe that the field is promptly screened inside the metal on a characteristic spatial scale given by the

https://doi.org/10.1021/acsphotonics.4c02612
ACS Photonics 2025, 12, 2137−2150

Wigner−Seitz radius (for the present system 3.02 au) as can be inferred from the near equivalence of the ground state and the dynamical potential at negative x.

Obviously, for the narrow 1 nm gap, an electron injected in the junction will interact with the optical field only briefly since it will be quickly directed toward the opposite metal surface by an attractive potential at the metal/vacuum interface that overrides the potential induced even by the strong (10 V/nm) optical field. This is in contrast to a broad gap (such as the 6 nm gap shown in Figure 2d) where an electron moving in the junction will explore the variation of the optical field over a long propagation distance range, making the situation close to the one encountered in the photoemission from a metal surface. In Figure S2 of the Supporting Information, we further support this discussion by comparing the field induced by the optical pulse and the field owing to the metal/vacuum interface potential.

Dynamics of Electron Transport and Its Dependence on the CEP. The color maps of the x-component of the time-dependent electron current density in Figure 3 reveal the impact of the small size of the gap on the dynamics of electronic currents in 1−2 nm gaps (for a comparison with the wide 6 nm gap see Figure S3 of Supporting Information). The TDDFT calculations are performed for a single-cycle optical pulse with optimum CEP = π maximizing the electron transfer for a 1 nm gap. The top row of the color maps corresponds to the current density at the dimer axis $j_x(x, y = 0, t) = \hat{e}_x \cdot \mathbf{j}(x, y = 0, t)$. The bottom row of the color maps features $j_{\mathrm{L},x}(x, y = 0, t) = \hat{e}_x \cdot \mathbf{j}_{\mathrm{L}}(x, y = 0, t)$, i.e., the contribution to $j_x(x, y = 0, t)$ of the cylinder on the left side of the junction. The results are shown as a function of x-coordinate and time.

We start our discussion with the situation often considered in the literature where large E_g (here 16.4 and 14.5 V/nm) drives the optical field emission, allowing for an intuitive interpretation of the results. Common for both sizes of the gap shown in Figure 3a, an intense electron burst of sub-fs duration is injected into the junction from the left metal surface close to $t = 0$. This time instant corresponds to the main extremum of the optical field in the gap with a negative sign of the field. The electron current burst propagates in the positive direction of the x-axis (positive j_x) and crosses the gap on a time scale of ≈700 attoseconds (1 nm gap) and ≈1.4 fs (2 nm gap). This can be particularly clearly seen from the lower panels where only $j_{\mathrm{L},x}(x, y = 0, t)$ is shown. Indeed, for the upper panels, the moment when the main burst crosses the metal surface at the right side of the junction is masked by the less intense "secondary" electron burst emitted from this surface in the negative direction of the x-axis (negative j_x). The "secondary" electron bursts are triggered by the secondary field extrema at the positive half-periods at $t \approx \pm 2$ fs.

It is worth noting that the saturated colors at the metal/vacuum interfaces on both sides of the gap correspond to currents due to the polarization of each nanowire. Consequently, they vanish when the surface charge density is largest, i.e., at crests of the optical field. Most importantly, polarization currents do not lead to charge transport across the gap. There is approximately a $\pi/2$ phase shift between the gap currents and the polarization currents, similar to the shift reported in a recent work on near-field optical tunneling emission.[51]

Since the main electron burst crosses the 1 nm junction on a time-scale below 1/4 of the optical cycle, the electrons are continuously accelerated by the optical field of the same sign and cross the second interface, without experiencing quiver motion.[71] The quenching of the quiver motion has been reported in photoemission from sharp nanostructures[27,37,92,93] where it results from the spatial decay of the near fields. In the present situation, the optical field in the narrow metallic gap is homogeneous, and it is screened in the metal leads. Thus, the electron−field interaction is stopped when the transmitted electrons enter the metal on the opposite side of the gap. For the 2 nm wide junction, a longer crossing time results in slow electrons being affected by the change of the sign of the optical field in the gap and showing quiver motion. This is particularly well seen in the color map of $j_{\mathrm{L},x}(x, y = 0, t)$. An eventual electron rescattering from the parent or target metal surfaces cannot be detected on the scale of the main electron burst. While this process is behind the low-intensity, high-energy tail of the electron energy spectrum for optical field emission from metal surfaces,[3,4,6,7,22,26,30] its probability is too low to affect the net electron transport in the present system. Moreover, for the narrow 1 nm gap, the absence of a clear-cut separation between the asymptotic region and metal surfaces should also result in an ill-defined notion of the rescattering event.

In Figure 3a, we also display semi-classical trajectories calculated with the strong-field model (see ref 71 and Section SI11 for details). Three characteristic trajectories are shown: an electron trajectory with a small final kinetic energy with respect to the vacuum energy (black dotted line), a trajectory starting at the crest of the optical field (white line), and a trajectory of fast electrons with cutoff energies $\mathcal{E}(t^*) = 12.8$ eV (26.3 eV) for 1 nm (2 nm) gap (red dashed line). Here t^* is the time instant when the trajectory crosses the facing metal surface. Notice that these cutoff energies are slightly different from the adiabatic cutoff[71] $\mathcal{E} = E_g d_{\mathrm{gap}} - 4.5$ eV, indicating that the field in the gap varies during the electron travel and the adiabatic regime is not completely attained.

We note that all trajectories are "born" with a spatial displacement from the left metal surface into the gap, which we identify with the semi-classical tunnel exit of optical field emission. The emitted electrons quickly gain kinetic energy, indicated by a strong bending of the trajectory slope after the tunnel exit. After the bending, the trajectories agree well with the TDDFT electron current density map, with the field crest trajectory (white line) lining up with the current density maximum. This further corroborates the suppression of the quiver motion and near-instantaneous electron transport in the optical field emission regime for few-nm gaps.

For the multiphoton photoemission at a small E_g, the overall lower energies of the electrons in the gap are evidenced in Figure 3b by the longer propagation times of the electron bursts. Moreover, since polarization currents scale as $\propto E_g$ while the transport currents scale as $\propto E_g^{2n}$, the former gain in relative intensity. Aside from these differences, the main aspects of the dynamics of electron currents, and in particular direct crossing of the gap by photoemitted electrons, are very similar to those reported above for strong fields. As discussed previously,[23,43,70,94,95] this qualitative similarity stems to a large extent from the highly nonlinear character of photoemission where the main electron burst is emitted at the crest of the optical field close to $t = 0$.

https://doi.org/10.1021/acsphotonics.4c02612
ACS Photonics 2025, 12, 2137−2150

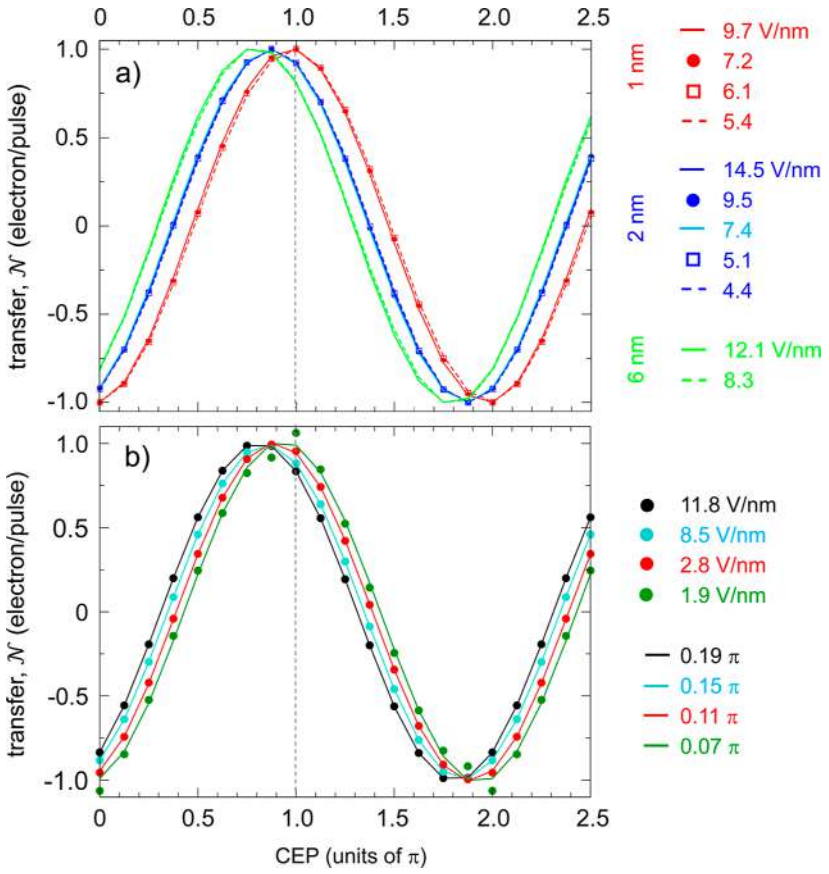

Figure 4. CEP dependence on electron transport. (a) Normalized net electron transfer $\mathcal{N}$ calculated with TDDFT as a function of the CEP of the single-cycle *x*-polarized optical pulse with frequency ω = 0.95 eV. Positive $\mathcal{N}$ corresponds to electrons transferred from the left to the right side of the gap along the positive direction of the *x*-axis. Results are shown for the 1 nm (red), 2 nm (blue), and 6 nm (green) gaps for various amplitudes of the optical field in the gap E_g measured in V/nm. The color code is explained in the legend. (b) Normalized net electron transfer $\mathcal{N}$ across a 1 nm gap calculated with TDDFT as a function of the CEP of the single-cycle *x*-polarized optical pulse with frequency ω = 2.0 eV. Results are shown for various amplitudes of the optical field in the gap E_g measured in V/nm. Circles: TDDFT results; lines of the corresponding color: fit by the $\cos(\varphi - [\pi - \delta\varphi])$ dependence, where $\delta\varphi$ is the optimum CEP offset from π given in the legend of the figure.

It is interesting to compare the results obtained here with those reported for vacuum gaps of widths of 3 nm and above. For the very wide (tens of nanometers) gaps, the situation approaches photoemission from an individual metal surface. The released electrons are driven for a sufficiently long time solely by the optical field. This results in quiver trajectories and affects the CEP dependence of the photoemission and electron energy spectra.[3,4,40] The relevant parameter to describe the electron propagation is the quiver amplitude, $X_q = E_g/\omega^2$. When the size of the gap becomes smaller or comparable to X_q, the electrons cross the gap without experiencing quiver motion as demonstrated for a 3 nm gap in the optical field emission regime by Aguirregabiria et al.[96] Since $X_q \approx 1.4$ nm for E_g = 16.4 V/nm, the results shown in Figure 3a can be well explained by the above rule. Now, reducing the field strength leads to X_q = 0.5 nm for E_g = 6 V/nm and X_q = 0.3 nm for E_g = 4 V/nm. Based on the findings of Aguirregabiria et al.,[96] one would expect that for d_{gap} = 1 nm, most of the trajectories display the quiver motion for weak optical fields in the multiphoton regime. In sheer contrast, the TDDFT results in Figure 3b show that under these conditions the photoemitted electrons directly cross the gap without quiver motion. This apparent contradiction can be explained as follows.

In the optical field emission regime, the force exerted on the photoemitted electron by the strong field E_g drives the electron dynamics, and the effect of the field-free potential can be neglected. Most of the electrons directly cross the gap if $X_q \gtrsim d_{gap}$ or experience quiver motion if $X_q \lesssim 0.5\ d_{gap}$.[96] In the multiphoton regime, over an essential part of the 1 nm junction, the field created by the optical pulse is smaller than the field owing to the metal/vacuum interfaces as can be inferred from extrapolating results of Figures 2c and S2 of the Supporting Information to small E_g. Thus, it is the optical-field-free (ground-state) potential of the junction that determines electron transport. The quiver amplitude is not a relevant parameter anymore to characterize the electron transport in a 1 nm junction in the multiphoton regime. As follows from the slope of the $\mathcal{N}(E_g)$ dependence in Figure 2 and from the results reported in the next section, the energies of the photoemitted electrons are close to the top of the potential barrier of the junction (for a 1 nm gap, some of the electrons undergo classically forbidden under-the-barrier tunneling). When an electron crosses the potential barrier, it is attracted by the facing metal surface without the possibility of velocity reversal by the optical field. The electron transport in this situation is not associated with the quiver motion. Obviously, the arguments above also apply to the 2 nm gap, albeit to a lesser extent. For the wide gaps, the field-free interaction is essentially zero over a large region inside the gap so that the

https://doi.org/10.1021/acsphotonics.4c02612
ACS Photonics 2025, 12, 2137−2150

electron dynamics can be analyzed in terms of quiver amplitude for strong and weak optical fields.

Since photoemitted electrons cross the 1 nm gap without quiver motion, the condition for maximum positive electron transport to occur must correspond to CEP = π irrespective of the field strength; i.e., maximum transport corresponds to the maximum attainable field in the gap in the negative direction of the x-axis. This is fully supported by the TDDFT results in Figure 4a. The same CEP dependence of the net electron transfer with optimum CEP = π is obtained over a wide range of E_g corresponding to Keldysh parameters $0.7 \leq \gamma \leq 2.5$, i.e., from the multiphoton photoemission to the onset of the optical field emission regime. The optimum CEP = π for electron transport in narrow gaps was also reported recently[71] but only in the optical field emission regime.

We note that for the 2 nm gap, a slight ($\approx 0.1\pi$) offset of the optimal CEP is consistent with an appearance of the quiver motion for some of the electron trajectories. For the 6 nm gap, the quiver motion causes an offset of the optimum CEP by $\approx 0.2\pi$, close to $\approx 0.25\pi$ offset of the optimum CEP calculated for wider gaps[96] and for the photoemission from an individual metal surface.[19,21] Given the high nonlinearity and short duration of the pulse we do not reach the inversion of the optimum CEP at high fields as reported in other systems.[8,19,36]

To further illustrate the CEP dependence of the electron transfer in the optical field (large E_g)-driven regime or in the ground-state potential (small E_g)-driven regime, we performed TDDFT calculations using the single-cycle optical pulse defined in eq 1, where ω = 2 eV so that X_q = 0.2 nm for E_g = 12 V/nm, and X_q = 0.04 nm for E_g = 2 V/nm; i.e., the quiver amplitude is significantly smaller than the size of the gap over the entire range of field strengths encompassed here. Results are shown in Figure 4b. In full accord with the discussion above, we obtain that for the large E_g, the quiver effect results in an optimum CEP $\approx 0.8\pi$. However, for a small optical field, it is the ground-state tunneling barrier that determines the trajectories of the transferred electrons, and the optimum CEP tends to π. The electron transfer is direct (no quiver) despite X_q being 25 times smaller than the gap size.

To conclude this section, our results indicate that a device with a narrow metallic gap, even though representing fabrication challenges, could eventually be used for on-chip absolute CEP sensing of the few-cycle pulses within a broad intensity range without a systematic CEP offset. Here, a resonance condition with a plasmon mode of the dimer is not required. It is often used in devices with broad gaps to reach the strong-field emission regime[38,42,44] but leads to an unavoidable phase shift of the field in the gap as compared to the free-space transient. The advantage of the off-resonant excitation is also discussed in recent work where nanoantenna networks were used for single-shot phase detection.[45]

Acceleration of Photoemitted Electrons by the Induced Field in the Gap and Hot Electron Injection into Metallic Leads. The sub-fs time scale for optically induced electron transfer in narrow 1−2 nm size junctions profoundly affects the physics of the process and leads to consequences reaching beyond the CEP dependence of the net electron transport $\mathcal{N}$ discussed above. One of the major effects to expect is that for a crossing time below 1/4 of the optical cycle, the electron burst ejected from the "parent" lead and moving in the gap is continuously accelerated by the optical field of the same sign. The electrons crossing the metal/vacuum interface of the metal lead at the opposite side of the gap are then characterized by a non-thermal post-injection energy distribution. The electron transport is therefore associated with hot electron injection into metallic leads as has been recently discussed for the adiabatic strong field-driven tunneling regime.[71] Here we confirm this result by analyzing the characteristic energies of the transferred electrons from our TDDFT calculations. Using model approaches validated by comparison with TDDFT, we further obtain and discuss the evolution of the energy spectra of electrons injected into the metallic leads with the strength of the field in the gap and with gap size. The former is varied from the multiphoton to the strong field regime and the latter from 1 nm (quiver-free transfer) to 6 nm (photoemitted electrons follow quiver trajectories inside the gap).

Let us start our discussion considering the classical simple man's model[97−100] (also see Section SI10 of the Supporting Information). This model provides intuitive insights into electron dynamics and it is often used, e.g., for the description of the optical field emission from metals.[3,4,23] Within this model, an electron is released from the metal surface at time $t = t_0$ with zero kinetic momentum p. It then moves under the sole action of an electric field of the pulse so that $p(t^*) = A(t^*) - A(t_0)$, where t^* is the instant of time where an electron enters the facing metal surface, and the vector potential $A(t)$ is defined with $E_{gap}(t) = -\frac{dA}{dt}$. Let us assume a harmonic variation of the field in the gap. For an electron emitted at $t_0 = 0$, i.e., at the crest of the field ($A(t_0) = 0$), we obtain that if $t^* = \pi/2\omega$ (1/4 of the optical period), then the final electron energy $\mathcal{E} = \frac{1}{2}p(t^*)^2 = 2U_p$. At this point, it is worth stressing that for the emission from a metal surface, this is the cutoff energy for the direct electrons,[3,4] while in the present case, this is the energy of the main electron burst. As another important remark, since for the photoemission from an individual metal surface (which is nothing else than the limiting case of an extremely broad gap) $A(t^* \to \infty) = 0$, the final energy of the majority of electrons within the main burst emitted at the crest of the optical field will be close to zero.

In the case of adiabatic tunneling, if the variation of the field in the gap on a time scale of the electron transport can be neglected so that $E_{gap}(t^*) = E_{gap}(t_0)$, an electron energy with respect to the vacuum level can be obtained from $\mathcal{E} = E_{gap}(t_0)d_{gap} - \Phi$. The maximum attainable electron energy (an energy cutoff of the transmitted electron energy spectrum) is given by $\mathcal{E}_{max} = E_g d_{gap} - \Phi$.[71]

In our system, the energy spectra of the electrons transferred through the gap between the nanowires are difficult to extract from the TDDFT as we discuss in Section SI4 of the Supporting Information. The current density maps calculated with TDDFT can be used nonetheless to obtain the characteristic energies of transmitted electrons (see Section SI4). For the 1 nm gap and E_g = 16.4 V/nm, we estimate the energy of the electrons at the maximum of the main burst as $\mathcal{E}_{peak} \approx 8$ eV and the lowest electron energy as $\mathcal{E}_{slow} \approx -2.4$ eV (energies are given with respect to the vacuum level). This latter case corresponds to the photon-assisted tunneling with energy below the top of the tunneling barrier (Figure 1b). Similarly, for the 2 nm gap and E_g = 14.3 V/nm, we obtain $\mathcal{E}_{peak} \approx 14$ eV and the lowest electron energy $\mathcal{E}_{slow} \approx -3.9$ eV. Thus, in full accord with intuitive arguments, the TDDFT results indicate that for the 1 and 2 nm gaps, the optically induced current is associated with energetic electron injection

https://doi.org/10.1021/acsphotonics.4c02612
ACS Photonics 2025, 12, 2137−2150

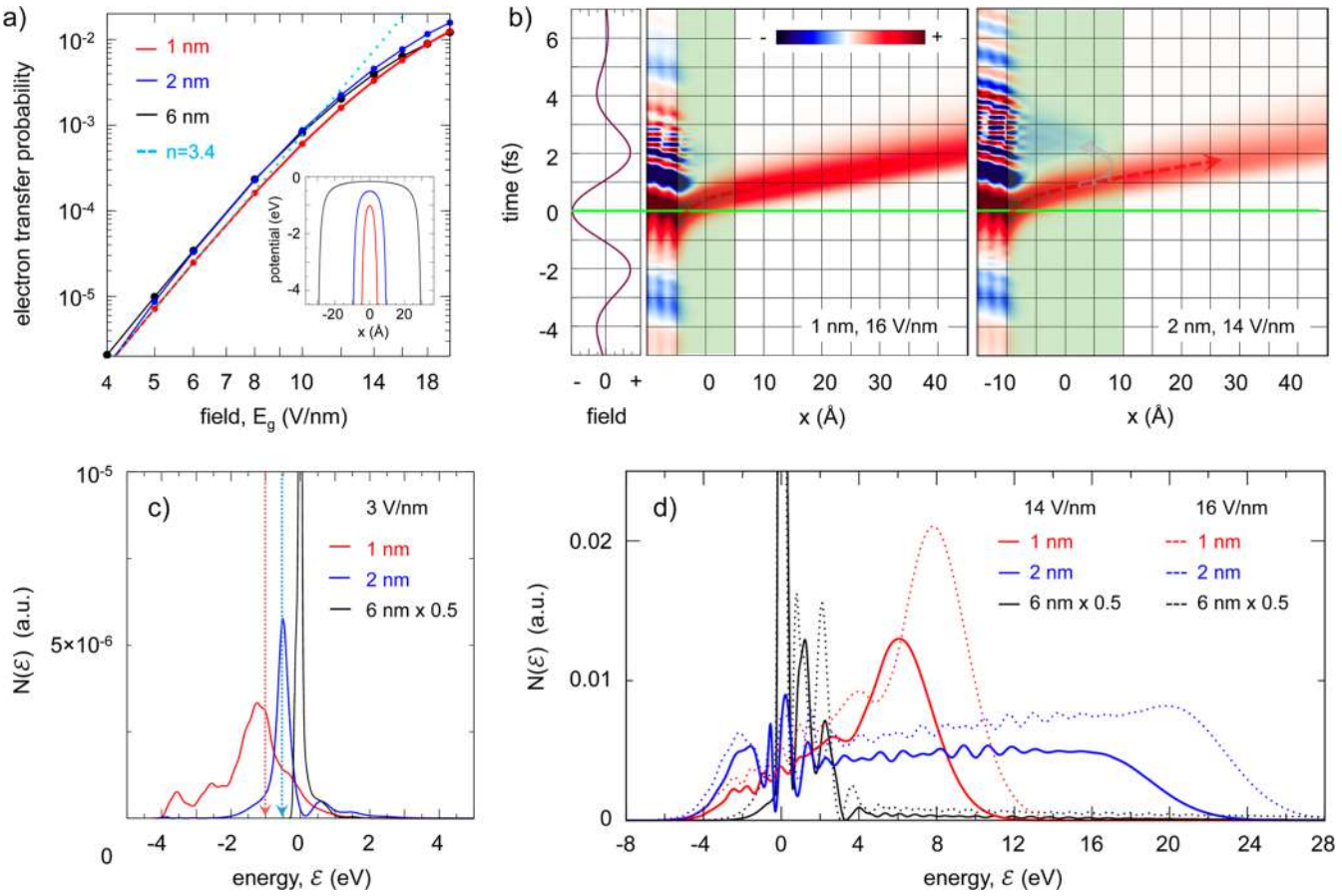

Figure 5. Model 1D WPP study of the optically induced electron transfer between metal leads separated by a narrow vacuum gap. The electric field of the CEP = π single-cycle pulse is given by eq 4. (a) Probability of electron transfer across the 1 nm (red), 2 nm (blue), and 6 nm (black) gaps. Initially, an electron occupies an orbital with Fermi energy in the left lead. WPP results are shown with solid lines as a function of the field amplitude in the gap E_g. Dashed light blue line: fit by the E_g^{2n} dependence with n, the number of absorbed photons. The inset shows the x-coordinate dependence of the model potential in the gap region. Energy zero corresponds to the vacuum level. (b) 2D maps of the normalized electron current density $j_x(x, t)$ induced by the single-cycle pulse with an optical field amplitude E_g = 16 V/nm (E_g = 14 V/nm) in the 1 nm (2 nm) gap. The WPP results are shown as a function of the x-coordinate (horizontal axis) and time (vertical axis). The color code is given in the inset. The line plot at the left shows the time evolution of the electric field in the gap. The shaded green region of x-coordinates indicates the junction. Red dashed arrows indicate a flow of electrons transferred into the right electrode, gray arrow indicates the quiver motion. The horizontal green line marks the instant of time when the field in the gap reaches its maximum value. (c,d) Energy spectrum of the electron transferred across the 1, 2, and 6 nm gaps into the right lead for an optical field amplitude E_g = 3 V/nm (c), as well as 14 V/nm and 16 V/nm (d). Results are shown as a function of electron energy $\mathcal{E}$ measured with respect to the vacuum level. Vertical arrows of the corresponding color in panel (c) indicate the energy of the top of the potential barrier for the 1 and 2 nm gap (also see the inset of panel a). For further details, see the legends.

into the metallic leads. In the examples discussed above, when crossing the metal/vacuum interface, *an essential part of transferred electrons* reach energies of $\mathcal{E}_{peak} + \Phi > 12$ eV with respect to the Fermi level which corresponds to an absorption of as much as 12 photons.

To gain further insights, we perform a model one-dimensional (1D) study of the optically induced one-electron transport through the potential barrier between free-electron metals. The method employed here is based on the solution of the time-dependent Schrödinger equation and it is often used to grasp the robust physics underlying the optical pulse interaction with metals and electron transport in metallic gaps.[23,34,59,70,71,95] The system is described by the model potential $V_{1D}(x)$ (see Sections SI5 and SI8 for details). Initially, an electron "active" in the optically induced transport occupies an orbital with Fermi energy $\mathcal{E}_F = -\Phi + V_{1D}(0)$ in the metal at the left of the junction. With this choice of $\mathcal{E}_F$, we enforce the height of the tunneling barrier to be close to that in the TDDFT calculations. The wave packet propagation (WPP) technique[101,102] (see Section SI8 of the Supporting Information) is used to calculate the time-dependent wave function of an "active" electron in the presence of the optical field. The screening of the latter inside the metal mimics the screening calculated with TDDFT. The energy spectrum of the transferred electron $N(\mathcal{E})$ is rigorously obtained using the virtual detector method.[103]

The model character of the potentials driving the electron dynamics, and in particular of the screening of the induced field, as well as the representation of the entire conduction band by a single orbital, calls for validation of the WPP approach. In this respect, the WPP results shown in Figure 5 confirm that the simple one-electron-model approach remarkably captures many aspects of the many-body self-consistent TDDFT calculations. Thus, the electron transfer probability per single-cycle pulse calculated with WPP as a function of E_g (Figure 5a) features qualitatively the same trends as in the TDDFT study (Figure 2b) with an electron transfer very

https://doi.org/10.1021/acsphotonics.4c02612
ACS Photonics 2025, 12, 2137−2150

similar for different gap sizes and dominated by transitions with electron energies close to the top of the barrier. The somewhat lower order of nonlinearity as compared to the TDDFT can be explained by the single electron state at energy $-\Phi$ below the barrier considered in WPP, while in the TDDFT, it is the band of states with binding energies $\geq \Phi$ that is involved in the optically induced current. Similarly, the dynamics of the electron current calculated with WPP (Figure 5b) closely resembles the many-body results for the left cylinder contribution to the electron current density $j_{L,x}(x, y = 0, t)$ (Figure 3a). Once injected into the right lead with constant potential inside the free-electron metal, the electron burst follows a straight-line trajectory and broadens because of the dispersion, which is also very similar to the extended many-body results discussed in Section SI4.

In Figure 5c,d we show the energy spectra of the transferred electron calculated with WPP for d_{gap} = 1, 2, and 6 nm, using the field in the gap E_g = 3 V/nm (Figure 5c), E_g = 14 V/nm, and E_g = 16 V/nm (Figure 5d). Results are shown as a function of transferred electron energy $\mathcal{E}$ measured in the right lead with respect to the vacuum level. In the multiphoton regime (Figure 5c), the energy spectra for the 6 and 2 nm gaps are dominated by the low electron energies close to the top of the barrier (see the inset of panel (a) pointing at the dominance of the over-the-barrier transfer. For the wide 6 nm gap, the top of the tunneling barrier, given by the potential in the middle of the gap, corresponds to the vacuum level $V_{1D}(x = 0) = 0$. This is while for the 1 and 2 nm gaps, $V_{1D}(x = 0)$ is found at a negative energy because of the image charge interaction accounted for in the model potential $V_{1D}(x)$ (Sections SI5 and SI8). Interestingly, for the narrow 1 nm gap one clearly observes the peaks at $\mathcal{E}_F + 2\omega$ and $\mathcal{E}_F + 3\omega$ owing to the photon-assisted tunneling at energies below the top of the barrier in full accord with conclusions drawn from the analysis of TDDFT results. Albeit significantly smaller, the contribution of the below-the-barrier tunneling is also apparent in the electron energy spectra calculated for a 2 nm gap.

In the optical field emission regime, the electron dynamics in the wide d_{gap} = 6 nm gap is characterized by the quiver motion of the emitted electrons resulting in an electron energy spectrum dominated by low electron energies similar to that from an individual metal surface.[3,4] In sheer contrast, the fs electron travel time through the narrow 1 and 2 nm gaps results in continuous electron acceleration along the path inside the gap with energetic electrons injection into the right lead. For the 1 nm gap, the high electron energies dominate the spectrum with a maximum of ≈8 eV (≈6 eV) for E_g = 16 V/nm (14 V/nm). An energy cutoff ≈14 eV (≈12 eV) is somewhat higher than the adiabatic prediction $\mathcal{E}_{max} = E_g d_{gap} + \mathcal{E}_F$ obtained within the analytical strong-field model.[71] This is because in the present situation, the field obviously varies on the time scale of electron transport so that the adiabatic conditions are not completely fulfilled. As we further show in Section SI11, the electron energy spectra calculated with WPP can be nicely reproduced using semi-classical trajectories calculated with the strong-field model.[71] For the 2 nm gap, part of the electron trajectories are affected by the reversal of the sign of the field, we then obtain a rather flat energy distribution extending up to the cutoff energy $\mathcal{E}_{max} \approx 28$ eV (24 eV) for E_g = 16 V/nm (14 V/nm).

It is worth noting that the quenching of the quiver motion in the optical field emission regime with an increase of the high-energy part of the energy spectrum of emitted electrons has been also reported for sharp metallic structures.[27,37,92,93] However, while in the present system, the spatial variation of the induced field is small inside the gap and the electron−field interaction is promptly stopped because of the field screening in metal, for a metallic tip, the effect stems from the decay of the near-field with increasing the distance from the metal. The quiver quenching is observed when the characteristic spatial scale of the near field variation given by the tip radius ($\gtrsim$10 nm) is comparable to or shorter than the quiver amplitude. As a consequence, an optical wavelength of 2.6 μm and above (Keldysh parameter γ within the 0.1−0.3 range) was used by Herink et al.[92] to reveal the quenching of the quiver motion from the analysis of the cutoff energy. When light field parameters are adapted to match our case, the high-energy contribution to the electron energy spectrum reported by Herink et al. is comparatively small.

All aspects considered, the energy spectra calculated with WPP nicely agree with the electron energy analysis from the TDDFT results reported above. The bulk of our results brings solid evidence for hot electron injection into metallic leads accompanying the optically induced electron transport across nanometer-sized metallic gaps in the strong-field regime. Since the mean free path of some 10 eV electrons in metals is below 1 nm,[104,105] once injected into the metallic leads, the energetic electrons will be promptly thermalized by exchanging their energy with valence electrons of the metal (fs time scales) and phonons (ps time scales).[106,107] The intrinsic losses due to inelastic electron−electron interactions cannot be captured within the TDDFT-ALDA scheme,[108−110] and the description of the evolution of the non-equilibrium electron energy distribution in the metal requires a different theoretical framework.[107,111−115] This said, to the best of our knowledge, the thermalization of an electron energy distribution that underwent excitation by a single-cycle optical pulse has not been studied even for an individual nanoparticle, which shows a challenging aspect of this problem. The fate of the injected electrons is therefore beyond the scope of the present study.

SUMMARY, CONCLUSIONS, AND OUTLOOK

In conclusion, using the many-body TDDFT, 1D model single-electron WPP calculations, and a semiclassical strong-field model,[71] we theoretically studied electron transport induced by single-cycle optical pulses at a 1300 nm wavelength (0.95 eV) in few-nm gaps between metal surfaces of relevance in nanoscale-transport configurations such as STM junctions, MIM structures, or optical antennas produced by electro-migration.

We focused our study on symmetric gaps with no applied bias so that it is solely the time-dependent field of the optical transient that breaks the symmetry and allows for net electron transport.

The 1−2 nm gaps represent an interesting system where (i) the direct tunneling and the single-photon-assisted tunneling are still small so that the optically induced electron transport is dominated by electrons with energies close to the top of the potential barrier separating metals, and (ii) the electrons cross the gap on sub-fs time scales without experiencing the reversal of their propagation direction by the optical field.

Despite different emission probabilities and different electron energies, the TDDFT results show qualitatively similar dynamics of photoemitted electrons both in the multiphoton regime and in the optical field emission regime,

https://doi.org/10.1021/acsphotonics.4c02612
ACS Photonics 2025, 12, 2137−2150

with electron bursts injected into the gap at crests of the optical field. For a 1 nm wide gap, the same CEP dependence of the net electron transfer per optical pulse with optimal CEP = π is obtained for Keldysh parameters in a wide range of $0.7 \leq \gamma \leq 2.5$. This effect is analyzed in terms of the transport dominated by the optical field (optical field emission regime) or by the ground-state potential barrier (multiphoton emission). It can be of interest for the development of devices with few-nanometer gaps for on-chip determination of absolute CEP without the need for any additional plasmonic field enhancement in the gap.

We have demonstrated that for the strong optical field in the gap, the sub-fs electron travel times through the narrow 1 and 2 nm gaps are associated with continuous acceleration of the electrons by the optical field of the same polarity. This allows for CEP-controlled sub-fs injection of energetic (hot) electrons into the metal leads. We show that under certain conditions, the high-energy contribution can dominate the energy spectra of the transferred electrons. This result is in sheer contrast with optical field-induced electron transport in wide gaps or with the optical field emission from metal surfaces dominated by low-energy direct electrons. Further exalted by a plasmon resonance of a device, this effect could potentially be exploited for hot-electron-induced processes with the possibility of CEP control.

Our results are firmly based on the robust physics of electron excitation, emission, and transport across the vacuum gap. We believe that they will provide a solid benchmark for theoretical studies aimed at supporting the engineering of petahertz optoelectronic devices with narrow metallic gaps. Moreover, the insights obtained in this work can contribute to the development of scanning probe devices that combine the atomic-scale spatial resolution associated with narrow metallic junctions with the sub-fs time resolution offered by single-cycle optical pulses.

■ ASSOCIATED CONTENT

Supporting Information

The Supporting Information is available free of charge at https://pubs.acs.org/doi/10.1021/acsphotonics.4c02612.

Theoretical approaches used here and their additional results including time-dependent density functional theory (TDDFT) calculations for the cylinder dimer; optically induced electron currents for 1, 2, and 6 nm gaps; additional results on the analysis of the quiver motion and CEP dependence of electron transfer; evaluation of energies of the transferred electrons from the TDDFT results; potential barrier in the gap; role of the image potential; possibility to account for its effect by performing the TDDFT calculations with lower work function of the metal; TDDFT results for jellium metal with a work function of gold; effect of the symmetry breaking on the optically induced electron transport with an example of a dc bias applied across the gap; wave packet propagation calculations of the optically induced electron transport in a one-dimensional (1D) model system considering a single active electron; CEP dependence of the electron transport calculated with WPP; simple man's model analysis of the electron energy spectra; analytical strong field model and semiclassical electron trajectories; and effect of the plasmon ringing (PDF)

■ AUTHOR INFORMATION

Corresponding Author

Andrei G. Borisov − *Institut des Sciences Moléculaires d'Orsay (ISMO), UMR 8214, CNRS, Université Paris-Saclay, Orsay Cedex 91405, France; Donostia International Physics Center, Donostia 20018, Spain;* orcid.org/0000-0003-0819-5028; Email: andrei.borissov@universite-paris-saclay.fr

Authors

Boyang Ma − *Department of Physics, Solid State Institute, and The Helen Diller Quantum Center, Technion—Israel Institute of Technology, Haifa 32000, Israel*

Mario Zapata-Herrera − *Donostia International Physics Center, Donostia 20018, Spain;* orcid.org/0000-0001-5607-3194

Antton Babaze − *Donostia International Physics Center, Donostia 20018, Spain; Materials Physics Center, CSIC-UPV/EHU, Donostia 20018, Spain; School of Architecture, UPV/EHU, Donostia 20018, Spain;* orcid.org/0000-0002-9775-062X

Michael Krüger − *Department of Physics, Solid State Institute, and The Helen Diller Quantum Center, Technion—Israel Institute of Technology, Haifa 32000, Israel;* orcid.org/0000-0002-6188-9179

Javier Aizpurua − *Donostia International Physics Center, Donostia 20018, Spain; Department of Electricity and Electronics, FCT-ZTF, UPV/EHU, Leioa 48940, Spain; IKERBASQUE, Basque Foundation for Science, Bilbao 48009, Spain;* orcid.org/0000-0002-1444-7589

Complete contact information is available at: https://pubs.acs.org/10.1021/acsphotonics.4c02612

Funding

B.M. and M.K. acknowledge funding from the European Union's Horizon 2020 research and innovation program under grant agreement No 853393-ERC-ATTIDA and from the Israel Science Foundation (ISF) under grant 1504/20, as well as partial financial support from the Helen Diller Quantum Center at the Technion. J.A. and M.Z.-H. acknowledge funding from the European Union's MICIU/AEI/10.13039/501100011033 and from "ERDF, EU A way of making Europe" through project PID2022-139579NB-I00, as well as funding from the Department of Education, Research, and Universities of the Basque Government through project No. IT1526-22.

Notes

The authors declare no competing financial interest.

■ ACKNOWLEDGMENTS

A.G.B. gratefully acknowledges the warm hospitality of the Donostia International Physics Center (DIPC). Discussions with Y. Sivan are gratefully acknowledged.

■ REFERENCES

(1) Milošević, D. B.; Paulus, G. G.; Bauer, D.; Becker, W. Above-threshold ionization by few-cycle pulses. *J. Phys. B: At., Mol. Opt. Phys.* **2006**, *39*, R203.

(2) Becker, W.; Grasbon, F.; Kopold, R.; Milošević, D. B.; Paulus, G. G.; Walther, H. Above-Threshold Ionization: From Classical Features to Quantum Effects. In *Advances In Atomic, Molecular, and Optical Physics*; Bederson, B., Walther, H., Eds.; Academic Press, 2002; Vol. *48*, pp 35−98.

(3) Krüger, M.; Lemell, C.; Wachter, G.; Burgdörfer, J.; Hommelhoff, P. Attosecond physics phenomena at nanometric tips. *J. Phys. B: At., Mol. Opt. Phys.* **2018**, *51*, 172001.
(4) Dombi, P.; Pápa, Z.; Vogelsang, J.; Yalunin, S. V.; Sivis, M.; Herink, G.; Schäfer, S.; Groß, P.; Ropers, C.; Lienau, C. Strong-field nano-optics. *Rev. Mod. Phys.* **2020**, *92*, 025003.
(5) Park, D. J.; Ahn, Y. H. Ultrashort field emission in metallic nanostructures and low-dimensional carbon materials. *Advances in Physics: X* **2020**, *5*, 1726207.
(6) Dienstbier, P.; Seiffert, L.; Paschen, T.; Liehl, A.; Leitenstorfer, A.; Fennel, T.; Hommelhoff, P. Tracing attosecond electron emission from a nanometric metal tip. *Nature* **2023**, *616*, 702−706.
(7) Kim, H. Y.; Garg, M.; Mandal, S.; Seiffert, L.; Fennel, T.; Goulielmakis, E. Attosecond field emission. *Nature* **2023**, *613*, 662−666.
(8) Chelkowski, S.; Bandrauk, A. D. Sensitivity of spatial photoelectron distributions to the absolute phase of an ultrashort intense laser pulse. *Phys. Rev. A* **2002**, *65*, 061802.
(9) Paulus, G. G.; Grasbon, F.; Walther, H.; Villoresi, P.; Nisoli, M.; Stagira, S.; Priori, E.; De Silvestri, S. Absolute-phase phenomena in photoionization with few-cycle laser pulses. *Nature* **2001**, *414*, 182−184.
(10) Sayler, A. M.; Arbeiter, M.; Fasold, S.; Adolph, D.; Möller, M.; Hoff, D.; Rathje, T.; Fetić, B.; Milošević, D. B.; Fennel, T.; Paulus, G. G. Accurate determination of absolute carrier-envelope phase dependence using photo-ionization. *Opt. Lett.* **2015**, *40*, 3137−3140.
(11) Zherebtsov, S.; et al. Controlled near-field enhanced electron acceleration from dielectric nanospheres with intense few-cycle laser fields. *Nat. Phys.* **2011**, *7*, 656−662.
(12) Zherebtsov, S.; Süßmann, F.; Peltz, C.; Plenge, J.; Betsch, K. J.; Znakovskaya, I.; Alnaser, A. S.; Johnson, N. G.; Kübel, M.; Horn, A. Carrier-envelope phase-tagged imaging of the controlled electron acceleration from SiO2 nanospheres in intense few-cycle laser fields. *New J. Phys.* **2012**, *14*, 075010.
(13) Passig, J.; Zherebtsov, S.; Irsig, R.; Arbeiter, M.; Peltz, C.; Göde, S.; Skruszewicz, S.; Meiwes-Broer, K.-H.; Tiggesbäumker, J.; Kling, M. F.; Fennel, T. Nanoplasmonic electron acceleration by attosecond-controlled forward rescattering in silver clusters. *Nat. Commun.* **2017**, *8*, 1181.
(14) Higuchi, T.; Heide, C.; Ullmann, K.; Weber, H. B.; Hommelhoff, P. Light-field-driven currents in graphene. *Nature* **2017**, *550*, 224−228.
(15) Hanus, V.; Fehér, B.; Csajbók, V.; Sándor, P.; Pápa, Z.; Budai, J.; Wang, Z.; Paul, P.; Szeghalmi, A.; Dombi, P. Carrier-envelope phase on-chip scanner and control of laser beams. *Nat. Commun.* **2023**, *14*, 5068.
(16) Kruchinin, S. Y.; Krausz, F.; Yakovlev, V. S. Colloquium: Strong-field phenomena in periodic systems. *Rev. Mod. Phys.* **2018**, *90*, 021002.
(17) Paasch-Colberg, T.; Kruchinin, S. Y.; Sağlam, Ö.; Kapser, S.; Cabrini, S.; Muehlbrandt, S.; Reichert, J.; Barth, J. V.; Ernstorfer, R.; Kienberger, R.; Yakovlev, V. S.; Karpowicz, N.; Schiffrin, A. Sub-cycle optical control of current in a semiconductor: from the multiphoton to the tunneling regime. *Optica* **2016**, *3*, 1358−1361.
(18) Schiffrin, A.; et al. Controlling dielectrics with the electric field of light. *Nature* **2013**, *493*, 70−74.
(19) Lemell, C.; Tong, X.-M.; Krausz, F.; Burgdörfer, J. Electron emission from metal surfaces by ultrashort pulses: Determination of the carrier-envelope phase. *Phys. Rev. Lett.* **2003**, *90*, 076403.
(20) Apolonski, A.; Dombi, P.; Paulus, G. G.; Kakehata, M.; Holzwarth, R.; Udem, T.; Lemell, C.; Torizuka, K.; Burgdörfer, J.; Hänsch, T. W.; Krausz, F. Observation of light-phase-sensitive photoemission from a metal. *Phys. Rev. Lett.* **2004**, *92*, 073902.
(21) Dombi, P.; Apolonski, A.; Lemell, C.; Paulus, G. G.; Kakehata, M.; Holzwarth, R.; Udem, T.; Torizuka, K.; Burgdörfer, J.; Hänsch, T. W.; Krausz, F. Direct measurement and analysis of the carrier-envelope phase in light pulses approaching the single-cycle regime. *New J. Phys.* **2004**, *6*, 39.
(22) Dombi, P.; Irvine, S. E.; Rácz, P.; Lenner, M.; Kroó, N.; Farkas, G.; Mitrofanov, A.; Baltuška, A.; Fuji, T.; Krausz, F.; Elezzabi, A. Y. Observation of few-cycle, strong-field phenomena in surface plasmon fields. *Opt. Express* **2010**, *18*, 24206−24212.
(23) Yalunin, S. V.; Gulde, M.; Ropers, C. Strong-field photoemission from surfaces: Theoretical approaches. *Phys. Rev. B* **2011**, *84*, 195426.
(24) Bormann, R.; Gulde, M.; Weismann, A.; Yalunin, S. V.; Ropers, C. Tip-enhanced strong-field photoemission. *Phys. Rev. Lett.* **2010**, *105*, 147601.
(25) Wachter, G.; Lemell, C.; Burgdörfer, J.; Schenk, M.; Krüger, M.; Hommelhoff, P. Electron rescattering at metal nanotips induced by ultrashort laser pulses. *Phys. Rev. B* **2012**, *86*, 035402.
(26) Krüger, M.; Schenk, M.; Hommelhoff, P. Attosecond control of electrons emitted from a nanoscale metal tip. *Nature* **2011**, *475*, 78−81.
(27) Piglosiewicz, B.; Schmidt, S.; Park, D. J.; Vogelsang, J.; Groß, P.; Manzoni, C.; Farinello, P.; Cerullo, G.; Lienau, C. Carrier-envelope phase effects on the strong-field photoemission of electrons from metallic nanostructures. *Nat. Photonics* **2014**, *8*, 37−42.
(28) Krüger, M.; Thomas, S.; Förster, M.; Hommelhoff, P. Self-probing of metal nanotips by rescattered electrons reveals the nano-optical near-field. *J. Phys. B: At., Mol. Opt. Phys.* **2014**, *47*, 124022.
(29) Thomas, S.; Krüger, M.; Förster, M.; Schenk, M.; Hommelhoff, P. Probing of optical near-fields by electron rescattering on the 1 nm scale. *Nano Lett.* **2013**, *13*, 4790−4794.
(30) Ahn, B.; Schötz, J.; Kang, M.; Okell, W. A.; Mitra, S.; Förg, B.; Zherebtsov, S.; Süßmann, F.; Burger, C.; Kübel, M.; et al. Attosecond-controlled photoemission from metal nanowire tips in the few-electron regime. *APL Photonics* **2017**, *2*, 036104.
(31) Hoff, D.; Krüger, M.; Maisenbacher, L.; Sayler, A. M.; Paulus, G. G.; Hommelhoff, P. Tracing the phase of focused broadband laser pulses. *Nat. Phys.* **2017**, *13*, 947−951.
(32) Lehr, M.; Foerster, B.; Schmitt, M.; Krüger, K.; Sönnichsen, C.; Schönhense, G.; Elmers, H.-J. Momentum distribution of electrons emitted from resonantly excited individual gold nanorods. *Nano Lett.* **2017**, *17*, 6606−6612.
(33) Dombi, P.; Hörl, A.; Rácz, P.; Márton, I.; Trügler, A.; Krenn, J. R.; Hohenester, U. Ultrafast strong-field photoemission from plasmonic nanoparticles. *Nano Lett.* **2013**, *13*, 674−678.
(34) Lovász, B.; Sándor, P.; Kiss, G.-Z.; Bánhegyi, B.; Rácz, P.; Pápa, Z.; Budai, J.; Prietl, C.; Krenn, J. R.; Dombi, P. Nonadiabatic nano-optical tunneling of photoelectrons in plasmonic near-fields. *Nano Lett.* **2022**, *22*, 2303−2308.
(35) Putnam, W. P.; Hobbs, R. G.; Keathley, P. D.; Berggren, K. K.; Kärtner, F. X. Optical-field-controlled photoemission from plasmonic nanoparticles. *Nat. Phys.* **2017**, *13*, 335−339.
(36) Keathley, P. D.; Putnam, W. P.; Vasireddy, P.; Hobbs, R. G.; Yang, Y.; Berggren, K. K.; Kärtner, F. X. Vanishing carrier-envelope-phase-sensitive response in optical-field photoemission from plasmonic nanoantennas. *Nat. Phys.* **2019**, *15*, 1128−1133.
(37) Park, D. J.; Piglosiewicz, B.; Schmidt, S.; Kollmann, H.; Mascheck, M.; Lienau, C. Strong field acceleration and steering of ultrafast electron pulses from a sharp metallic nanotip. *Phys. Rev. Lett.* **2012**, *109*, 244803.
(38) Rybka, T.; Ludwig, M.; Schmalz, M. F.; Knittel, V.; Brida, D.; Leitenstorfer, A. Sub-cycle optical phase control of nanotunnelling in the single-electron regime. *Nat. Photonics* **2016**, *10*, 667−670.
(39) Karnetzky, C.; Zimmermann, P.; Trummer, C.; Duque Sierra, C.; Wörle, M.; Kienberger, R.; Holleitner, A. Towards femtosecond on-chip electronics based on plasmonic hot electron nano-emitters. *Nat. Commun.* **2018**, *9*, 2471.
(40) Ludwig, M.; Aguirregabiria, G.; Ritzkowsky, F.; Rybka, T.; Marinica, D. C.; Aizpurua, J.; Borisov, A. G.; Leitenstorfer, A.; Brida, D. Sub-femtosecond electron transport in a nanoscale gap. *Nat. Phys.* **2020**, *16*, 341−345.
(41) Zimmermann, P.; Hötger, A.; Fernandez, N.; Nolinder, A.; Müller, K.; Finley, J. J.; Holleitner, A. W. Toward plasmonic tunnel

https://doi.org/10.1021/acsphotonics.4c02612
ACS Photonics 2025, 12, 2137−2150

gaps for nanoscale photoemission currents by on-chip laser ablation. *Nano Lett.* **2019**, *19*, 1172−1178.
(42) Yang, Y.; Turchetti, M.; Vasireddy, P.; Putnam, W. P.; Karnbach, O.; Nardi, A.; Kärtner, F. X.; Berggren, K. K.; Keathley, P. D. Light phase detection with on-chip petahertz electronic networks. *Nat. Commun.* **2020**, *11*, 3407.
(43) Shi, L.; Babushkin, I.; Husakou, A.; Melchert, O.; Frank, B.; Yi, J.; Wetzel, G.; Demircan, A.; Lienau, C.; Giessen, H.; Ivanov, M.; Morgner, U.; Kovacev, M. Femtosecond field-driven on-chip unidirectional electronic currents in nonadiabatic tunneling regime. *Laser Photonics Rev.* **2021**, *15*, 2000475.
(44) Bionta, M. R.; Ritzkowsky, F.; Turchetti, M.; Yang, Y.; Cattozzo Mor, D.; Putnam, W. P.; Kärtner, F. X.; Berggren, K. K.; Keathley, P. D. On-chip sampling of optical fields with attosecond resolution. *Nat. Photonics* **2021**, *15*, 456−460.
(45) Ritzkowsky, F.; Yeung, M.; Bebeti, E.; Gebert, T.; Matsuyama, T.; Budden, M.; Mainz, R. E.; Cankaya, H.; Berggren, K. K.; Rossi, G. M.; Keathley, P. D.; Kärtner, F. X. On-chip petahertz electronics for single-shot phase detection. *Nat. Commun.* **2024**, *15*, 10179.
(46) Yeung, M.; Chou, L.-T.; Turchetti, M.; Ritzkowsky, F.; Berggren, K. K.; Keathley, P. D. Lightwave-electronic harmonic frequency mixing. *Sci. Adv.* **2024**, *10*, No. eadq0642.
(47) Schoetz, J.; Wang, Z.; Pisanty, E.; Lewenstein, M.; Kling, M. F.; Ciappina, M. F. Perspective on petahertz electronics and attosecond nanoscopy. *ACS Photonics* **2019**, *6*, 3057−3069.
(48) Heide, C.; Keathley, P. D.; Kling, M. F. Petahertz electronics. *Nat. Rev. Phys.* **2024**, *6*, 648−662.
(49) Bian, K.; Gerber, C.; Heinrich, A. J.; Müller, D. J.; Scheuring, S.; Jiang, Y. Scanning probe microscopy. *Nat. Rev. Methods Primers* **2021**, *1*, 36.
(50) Müller, M. Imaging surfaces at the space-time limit: New perspectives of time-resolved scanning tunneling microscopy for ultrafast surface science. *Prog. Surf. Sci.* **2024**, *99*, 100727.
(51) Siday, T.; Hayes, J.; Schiegl, F.; Sandner, F.; Menden, P.; Bergbauer, V.; Zizlsperger, M.; Nerreter, S.; Lingl, S.; Repp, J.; Wilhelm, J.; Huber, M. A.; Gerasimenko, Y. A.; Huber, R. All-optical subcycle microscopy on atomic length scales. *Nature* **2024**, *629*, 329−334.
(52) Yoshida, S.; Hirori, H.; Tachizaki, T.; Yoshioka, K.; Arashida, Y.; Wang, Z.-H.; Sanari, Y.; Takeuchi, O.; Kanemitsu, Y.; Shigekawa, H. Subcycle transient scanning tunneling spectroscopy with visualization of enhanced terahertz near field. *ACS Photonics* **2019**, *6*, 1356−1364.
(53) Arashida, Y.; Mogi, H.; Ishikawa, M.; Igarashi, I.; Hatanaka, A.; Umeda, N.; Peng, J.; Yoshida, S.; Takeuchi, O.; Shigekawa, H. Subcycle mid-infrared electric-field-driven scanning tunneling microscopy with a time resolution higher than 30 fs. *ACS Photonics* **2022**, *9*, 3156−3164.
(54) Wu, S.; Ogawa, N.; Ho, W. Atomic-scale coupling of photons to single-molecule junctions. *Science* **2006**, *312*, 1362−1365.
(55) Schröder, B.; Bunjes, O.; Wimmer, L.; Kaiser, K.; Traeger, G. A.; Kotzott, T.; Ropers, C.; Wenderoth, M. Controlling photocurrent channels in scanning tunneling microscopy. *New J. Phys.* **2020**, *22*, 033047.
(56) Martín Sabanés, N.; Krecinic, F.; Kumagai, T.; Schulz, F.; Wolf, M.; Müller, M. Femtosecond Thermal and Nonthermal Hot Electron Tunneling Inside a Photoexcited Tunnel Junction. *ACS Nano* **2022**, *16*, 14479−14489.
(57) Lin, C.; Krecinic, F.; Yoshino, H.; Hammud, A.; Pan, A.; Wolf, M.; Müller, M.; Kumagai, T. Continuous-wave multiphoton-induced electron transfer in tunnel junctions driven by intense plasmonic fields. *ACS Photonics* **2023**, *10*, 3637−3646.
(58) Luo, Y.; Neubrech, F.; Martin-Jimenez, A.; Liu, N.; Kern, K.; Garg, M. Real-time tracking of coherent oscillations of electrons in a nanodevice by photo-assisted tunnelling. *Nat. Commun.* **2024**, *15*, 1316.
(59) Garg, M.; Kern, K. Attosecond coherent manipulation of electrons in tunneling microscopy. *Science* **2020**, *367*, 411−415.
(60) Dasgupta, A.; Buret, M.; Cazier, N.; Mennemanteuil, M. M.; Chacon, R.; Hammani, K.; Weeber, J. C.; Arocas, J.; Markey, L.; des Francs, G. C.; Uskov, A.; Smetanin, I.; Bouhelier, A. Electromigrated electrical optical antennas for transducing electrons and photons at the nanoscale. *Beilstein J. Nanotechnol.* **2018**, *9*, 1964−1976.
(61) Ward, D. R.; Hüser, F.; Pauly, F.; Cuevas, J. C.; Natelson, D. Optical rectification and field enhancement in a plasmonic nanogap. *Nature Nanotechnol.* **2010**, *5*, 732−736.
(62) Lambe, J.; McCarthy, S. L. Light emission from inelastic electron tunneling. *Phys. Rev. Lett.* **1976**, *37*, 923−925.
(63) Parzefall, M.; Novotny, L. Light at the end of the tunnel. *ACS Photonics* **2018**, *5*, 4195−4202.
(64) Pommier, D.; Hufschmitt, Z.; Zhang, C.; Lai, Y.; Dujardin, G.; Le Moal, E.; Sauvan, C.; Greffet, J.-J.; Wang, J.; Boer-Duchemin, E. Nanoscale electrical excitation of surface plasmon polaritons with a nanoantenna tunneling junction. *ACS Photonics* **2023**, *10*, 2641−2649.
(65) Kimura, K.; Morinaga, Y.; Imada, H.; Katayama, I.; Asakawa, K.; Yoshioka, K.; Kim, Y.; Takeda, J. Terahertz-field-driven scanning tunneling luminescence spectroscopy. *ACS Photonics* **2021**, *8*, 982−987.
(66) Tucker, J. R.; Feldman, M. J. Quantum detection at millimeter wavelengths. *Rev. Mod. Phys.* **1985**, *57*, 1055−1113.
(67) Platero, G.; Aguado, R. Photon-assisted transport in semiconductor nanostructures. *Phys. Rep.* **2004**, *395*, 1−157.
(68) Feibelman, P. J. Surface electromagnetic fields. *Prog. Surf. Sci.* **1982**, *12*, 287−407.
(69) Marinica, D.; Kazansky, A.; Nordlander, P.; Aizpurua, J.; Borisov, A. G. Quantum plasmonics: Nonlinear effects in the field enhancement of a plasmonic nanoparticle dimer. *Nano Lett.* **2012**, *12*, 1333−1339.
(70) Luo, Y.; Zhang, P. Optical-field-induced electron emission in a dc-biased nanogap. *Phys. Rev. Appl.* **2022**, *17*, 044008.
(71) Ma, B.; Krüger, M. Strong-field theory of attosecond tunneling microscopy. *Phys. Rev. Lett.* **2024**, *133*, 236901.
(72) Kim, S.; Schmude, T.; Burkard, G.; Moskalenko, A. S. Quasiclassical theory of non-adiabatic tunneling in nanocontacts induced by phase-controlled ultrashort light pulses. *New J. Phys.* **2021**, *23*, 083006.
(73) Hu, Z.; Kwok, Y.; Chen, G.; Mukamel, S. Carrier-envelope-phase modulated currents in scanning tunneling microscopy. *Nano Lett.* **2021**, *21*, 6569−6575.
(74) Bhan, L.; Covington, C.; Varga, K. Signatures of atomic structure in subfemtosecond laser-driven electron dynamics in nanogaps. *Phys. Rev. B* **2022**, *105*, 085416.
(75) Chen, L.; Zhang, Y.; Chen, G.; Franco, I. Stark control of electrons along nanojunctions. *Nat. Commun.* **2018**, *9*, 2070.
(76) Perdew, J. P.; Tran, H. Q.; Smith, E. D. Stabilized jellium: Structureless pseudopotential model for the cohesive and surface properties of metals. *Phys. Rev. B* **1990**, *42*, 11627.
(77) Chulkov, E. V.; Silkin, V. M.; Echenique, P. M. Image potential states on metal surfaces: binding energies and wave functions. *Surf. Sci.* **1999**, *437*, 330−352.
(78) Krüger, M.; Schenk, M.; Hommelhoff, P.; Wachter, G.; Lemell, C.; Burgdörfer, J. Interaction of ultrashort laser pulses with metal nanotips: a model system for strong-field phenomena. *New J. Phys.* **2012**, *14*, 085019.
(79) Kohn, W.; Sham, L. J. Self-consistent equations including exchange and correlation effects. *Phys. Rev.* **1965**, *140*, A1133.
(80) Runge, E.; Gross, E. K. U. Density-functional theory for time-dependent systems. *Phys. Rev. Lett.* **1984**, *52*, 997.
(81) Marques, M. A. L.; Gross, E. K. U. Time-dependent density functional theory. *Annu. Rev. Phys. Chem.* **2004**, *55*, 427−455.
(82) Gunnarsson, O.; Lundqvist, B. Exchange and correlation in atoms, molecules, and solids by the spin-density-functional formalism. *Phys. Rev. B* **1976**, *13*, 4274.
(83) Stolz, A.; Berthelot, J.; Mennemanteuil, M.-M.; Colas des Francs, G.; Markey, L.; Meunier, V.; Bouhelier, A. Nonlinear photon-

https://doi.org/10.1021/acsphotonics.4c02612
ACS Photonics 2025, 12, 2137−2150

assisted tunneling transport in optical gap antennas. *Nano Lett.* **2014**, *14*, 2330−2338.
(84) Thon, A.; Merschdorf, M.; Pfeiffer, W.; Klamroth, T.; Saalfrank, P.; Diesing, D. Photon-assisted tunneling versus tunneling of excited electrons in metal-insulator-metal junctions. *Appl. Phys. A: Mater. Sci. Process.* **2004**, *78*, 189−199.
(85) Diesing, D.; Merschdorf, M.; Thon, A.; Pfeiffer, W. Identification of multiphoton induced photocurrents in metal-insulator-metal junctions. *Appl. Phys. B: Lasers Opt.* **2004**, *78*, 443−446.
(86) Zhou, S.; Guo, X.; Chen, K.; Cole, M. T.; Wang, X.; Li, Z.; Dai, J.; Li, C.; Dai, Q. Optical-field-driven electron tunneling in metal-insulator-metal nanojunction. *Advanced Science* **2021**, *8*, 2101572.
(87) Arai, K.; Okazaki, D.; Morichika, I.; Ashihara, S. All-solid-state optical-field-sensitive detector for sub-nanojoule pulses using metal-insulator hybrid nanostructure. *ACS Photonics* **2023**, *10*, 1702−1707.
(88) Krüger, M.; Schenk, M.; Förster, M.; Hommelhoff, P. Attosecond physics in photoemission from a metal nanotip. *J. Phys. B: At., Mol. Opt. Phys.* **2012**, *45*, 074006.
(89) Keldysh, L. V. Ionization in the field of a strong electromagnetic wave. *Sov. Phys. JETP* **1965**, *20*, 1307−1314.
(90) Swanwick, M. E.; Keathley, P. D.; Fallahi, A.; Krogen, P. R.; Laurent, G.; Moses, J.; Kärtner, F. X.; Velásquez-García, L. F. Nanostructured ultrafast silicon-tip optical field-emitter arrays. *Nano Lett.* **2014**, *14*, 5035−5043.
(91) Yanagisawa, H.; Schnepp, S.; Hafner, C.; Hengsberger, M.; Kim, D. E.; Kling, M. F.; Landsman, A.; Gallmann, L.; Osterwalder, J. Delayed electron emission in strong-field driven tunnelling from a metallic nanotip in the multi-electron regime. *Sci. Rep.* **2016**, *6*, 35877.
(92) Herink, G.; Solli, D. R.; Gulde, M.; Ropers, C. Field-driven photoemission from nanostructures quenches the quiver motion. *Nature* **2012**, *483*, 190−193.
(93) Li, C.; Zhou, X.; Zhai, F.; Li, Z.; Yao, F.; Qiao, R.; Chen, K.; Yu, D.; Sun, Z.; Liu, K.; Dai, Q. Quiver-quenched optical-field-emission from carbon nanotubes. *Appl. Phys. Lett.* **2017**, *111*, 133101.
(94) Hommelhoff, P.; Kealhofer, C.; Kasevich, M. A. Ultrafast electron pulses from a tungsten tip triggered by low-power femtosecond laser pulses. *Phys. Rev. Lett.* **2006**, *97*, 247402.
(95) Turchetti, M.; Bionta, M. R.; Yang, Y.; Ritzkowsky, F.; Candido, D. R.; Flatté, M. E.; Berggren, K. K.; Keathley, P. D. Impact of DC bias on weak optical-field-driven electron emission in nano-vacuum-gap detectors. *J. Opt. Soc. Am. B* **2021**, *38*, 1009−1016.
(96) Aguirregabiria, G.; Marinica, D.-C.; Ludwig, M.; Brida, D.; Leitenstorfer, A.; Aizpurua, J.; Borisov, A. G. Dynamics of electron-emission currents in plasmonic gaps induced by strong fields. *Faraday Discuss.* **2019**, *214*, 147−157.
(97) Lewenstein, M.; Balcou, P.; Ivanov, M. Y.; L'Huillier, A.; Corkum, P. B. Theory of high-harmonic generation by low-frequency laser fields. *Phys. Rev. A* **1994**, *49*, 2117−2132.
(98) Paulus, G. G.; Becker, W.; Nicklich, W.; Walther, H. Rescattering effects in above-threshold ionization: a classical model. *J. Phys. B: At., Mol. Opt. Phys.* **1994**, *27*, L703.
(99) Corkum, P. B. Plasma perspective on strong field multiphoton ionization. *Phys. Rev. Lett.* **1993**, *71*, 1994−1997.
(100) Paulus, G. G.; Becker, W.; Walther, H. Classical rescattering effects in two-color above-threshold ionization. *Phys. Rev. A* **1995**, *52*, 4043−4053.
(101) Chulkov, E. V.; Borisov, A. G.; Gauyacq, J. P.; Sánchez-Portal, D.; Silkin, V. M.; Zhukov, V. P.; Echenique, P. M. Electronic excitations in metals and at metal surfaces. *Chem. Rev.* **2006**, *106*, 4160−4206.
(102) Debiossac, M.; Zugarramurdi, A.; Lunca-Popa, P.; Momeni, A.; Khemliche, H.; Borisov, A. G.; Roncin, P. Transient quantum trapping of fast atoms at surfaces. *Phys. Rev. Lett.* **2014**, *112*, 023203.
(103) Sjakste, J.; Borisov, A. G.; Gauyacq, J. P.; Kazansky, A. K. Analysis of the population of continuum states in wave packet propagation calculations. *J. Phys. B: At., Mol. Opt. Phys.* **2004**, *37*, 1593.
(104) Ridzel, O. Y.; Astašauskas, V.; Werner, W. S. Low energy (1−100 eV) electron inelastic mean free path (IMFP) values determined from analysis of secondary electron yields (SEY) in the incident energy range of 0.1−10 keV. *J. Electron Spectrosc. Relat. Phenom.* **2020**, *241*, 146824.
(105) Le, D.-N.; Nguyen-Truong, H. T. Analytical formula for the electron inelastic mean free path. *J. Phys. Chem. C* **2021**, *125*, 18946−18951.
(106) Bauer, M.; Marienfeld, A.; Aeschlimann, M. Hot electron lifetimes in metals probed by time-resolved two-photon photoemission. *Prog. Surf. Sci.* **2015**, *90*, 319−376.
(107) Schirato, A.; Maiuri, M.; Cerullo, G.; Valle, G. D. Ultrafast hot electron dynamics in plasmonic nanostructures: experiments, modelling, design. *Nanophotonics* **2023**, *12*, 1−28.
(108) Ullrich, C. *Time-dependent Density-Functional Theory: Concepts and Applications; Oxford Graduate Texts*; Oxford University Press, 2019.
(109) Wijewardane, H. O.; Ullrich, C. A. Time-dependent Kohn-Sham theory with memory. *Phys. Rev. Lett.* **2005**, *95*, 086401.
(110) Vignale, G.; Kohn, W. Current-dependent exchange-correlation potential for dynamical linear response theory. *Phys. Rev. Lett.* **1996**, *77*, 2037−2040.
(111) Voisin, C.; Del Fatti, N.; Christofilos, D.; Vallée, F. Ultrafast electron dynamics and optical nonlinearities in metal nanoparticles. *J. Phys. Chem. B* **2001**, *105*, 2264−2280.
(112) Grua, P.; Morreeuw, J. P.; Bercegol, H.; Jonusauskas, G.; Vallée, F. Electron kinetics and emission for metal nanoparticles exposed to intense laser pulses. *Phys. Rev. B* **2003**, *68*, 035424.
(113) Besteiro, L. V.; Kong, X.-T.; Wang, Z.; Hartland, G.; Govorov, A. O. Understanding hot-electron generation and plasmon relaxation in metal nanocrystals: quantum and classical mechanisms. *ACS Photonics* **2017**, *4*, 2759−2781.
(114) Dubi, Y.; Sivan, Y. Hot electrons in metallic nanostructures-non-thermal carriers or heating? *Light:Sci. Appl.* **2019**, *8*, 89.
(115) Khurgin, J.; Bykov, A. Y.; Zayats, A. V. Hot-electron dynamics in plasmonic nanostructures: fundamentals, applications and overlooked aspects. *eLight* **2024**, *4*, 15.

https://doi.org/10.1021/acsphotonics.4c02612
ACS Photonics 2025, 12, 2137−2150